YALE
PEABODY
MUSEUM

P.O. BOX 208118 | NEW HAVEN CT 06520-8118 USA | PEABODY.YALE. EDU

## JOURNAL OF MARINE RESEARCH

The *Journal of Marine Research,* one of the oldest journals in American marine science, published important peer-reviewed original research on a broad array of topics in physical, biological, and chemical oceanography vital to the academic oceanographic community in the long and rich tradition of the Sears Foundation for Marine Research at Yale University.

An archive of all issues from 1937 to 2021 (Volume 1–79) are available through EliScholar, a digital platform for scholarly publishing provided by Yale University Library at https://elischolar.library.yale.edu/.

Requests for permission to clear rights for use of this content should be directed to the authors, their estates, or other representatives. The *Journal of Marine Research* has no contact information beyond the affiliations listed in the published articles. We ask that you provide attribution to the *Journal of Marine Research*.

Yale University provides access to these materials for educational and research purposes only. Copyright or other proprietary rights to content contained in this document may be held by individuals or entities other than, or in addition to, Yale University. You are solely responsible for determining the ownership of the copyright, and for obtaining permission for your intended use. Yale University makes no warranty that your distribution, reproduction, or other use of these materials will not infringe the rights of third parties.


This work is licensed under a Creative Commons Attribution-NonCommercial-ShareAlike 4.0 International License.
https://creativecommons.org/licenses/by-nc-sa/4.0/

*Journal of Marine Research, 47,* 717–746, 1989

Journal of
MARINE RESEARCH

Volume 47, Number 4

# The mythical thermohaline oscillator?

by Barry Ruddick[1] and Lingqi Zhang[1]

ABSTRACT

The system discussed by Stommel (1987) and Welander (1982), in which heating and evaporation at the surface of the ocean are balanced by vertical turbulent mixing, is studied analytically and numerically for mixing laws appropriate to salt fingers, rather than mechanical turbulence. Stommel and Welander found for mechanically-driven turbulent mixing that a limit cycle of $T$ and $S$ exists (that is, $T$ and $S$ oscillate) in the presence of steady forcing. We find that the usual salt finger parameterizations, in which salinity flux coefficient and buoyancy flux ratio decrease with increasing density ratio, do not allow a limit cycle. This result holds whether the flux parameterization is for an interface using the "4/3 power law" laboratory relationships or in terms of vertical gradients. Rather, all initial conditions either evolve to a steady balance or lead to the upper layer becoming denser than the lower layer and overturning. In addition, we find that commonly used mechanical turbulence parameterizations for eddy diffusivity vs. Richardson number do not vary rapidly enough to allow a limit cycle in the Stommel/Welander model, although recent observations of equatorial turbulence do.

Hence the possible existence of a limit oscillation in evaporatively-driven areas of the ocean depends critically on the type of vertical mixing which occurs, and on the precise form of its parameterization.

## 1. Introduction

Stommel (1961) pointed out that there are large areas of the world's oceans in which the upper waters are heated, and also suffer a net loss of evaporation over precipitation, so that the excess salt is left behind. He found that simple models of systems forced in such a manner can have multiple steady states in which the salt and heat fluxes can be balanced by mixing. Welander (1982) and Stommel (1986) found that for some

1. Department of Oceanography, Dalhousie University, Halifax, NS, Canada, B3H 4J1.

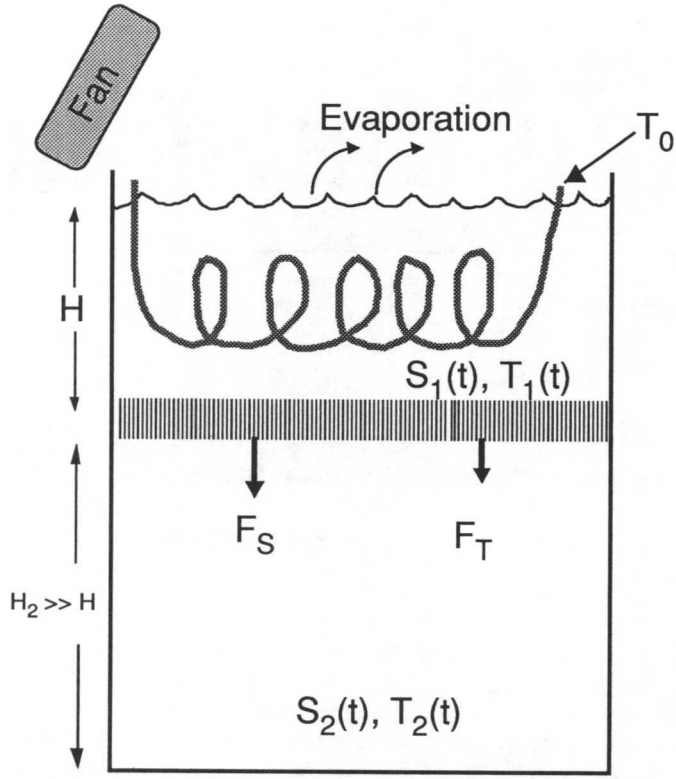


Figure 1. Diagram of the experimental configuration. A top layer is heated by a flow-through heat exchange coil, and evaporated by blowing warmed air over it. The lower layer is deep compared to the upper, and serves as a reservoir. Mixing at the interface, resulting in the salt ($F_S$) and heat ($F_T$) fluxes shown, primarily affects $S$ and $T$ in the top layer.

conditions, steady forcing can result in a cyclic, unsteady response. Stommel also noted that it was not likely that physical systems could be set up corresponding to his greatly simplified model.

It occurred to us that a system analogous to Stommel's model can indeed be set up in the laboratory, in which the vertical mixing is done by salt fingers. Such an experiment is shown in Figure 1, with a tall tank of salt water, stratified into two layers, an upper layer (#1) of depth $H$, and a lower layer (#2) that is so deep that we can ignore its $T$-$S$ variations. The upper layer is warmed by a heat exchange coil filled with water at temperature $T_0$, and has a fan blowing over it, evaporating water at a steady rate $w_E$. In the absence of external stirring, salt fingers will transport the salt and heat downward from the top layer at a rate that increases with decreasing density difference between the two layers. This type of mixing is thus analogous to that assumed by Stommel (1986) and Welander (1982), although the parameterization differs in detail.

The original motivation for this experiment was that it would be fun to set it up in the lab and demonstrate cyclic response of a fluid system to steady forcing. However, it might also be relevant to the study of the global atmospheric climate because of the following, rather tenuous, connections. The subtropical areas of the ocean to which Stommel refers correspond to the central waters studied by Schmitt (1981), in which the tendency for the $T$-$S$ relation to curve slightly is explained by a model of mixing due to salt fingers. His analysis gives strong support for the idea that the dominant vertical mixing is achieved by salt fingers, and not mechanical turbulence, which would result in a straight-line $T$-$S$ relation. As pointed out by Hamilton *et al.* (1989), the flux of salt in such regions is directly linked with the upward flux of nutrients into the euphotic zone, and hence with the new biological production, fixation of carbon, and the consequent uptake of $CO_2$ from the atmosphere. Some dynamical systems which oscillate under steady forcing can become chaotic under periodic forcing. There is, therefore, the possibility of a feedback link between atmospheric $CO_2$ and evaporation over the subtropical oceans, and the further possibility that the nonlinearities in the system could allow chaotic behavior.

When the heater and fan were turned on, the system *didn't* oscillate, but gave a stable, steady response. We therefore decided to investigate the problem theoretically, to see if there was a parameter range that was conducive to oscillation. As we will show below, no oscillations are possible when fluxes are parameterized in a manner suitable for salt fingers.

In the next section, we review Stommel's (1986) and Welander's (1982) models, to describe the mechanism of oscillation, and we note that the vertical distribution of salinity and temperature is such that the vertical mixing may be dominated by salt finger mixing. We then, in Section 3, analyze the system under the assumption that the vertical mixing is entirely due to salt fingers, and that the "4/3 flux laws" apply. As found in the lab, the parameterization of mixing by salt fingers does not allow the system to oscillate. Rather, the system either evolves toward a steady state, or leads to the upper layer becoming more dense than the lower and overturning. In Section 4 we investigate plausible forms of salt finger flux parameterizations in terms of vertical gradients of temperature and salinity, and find similar results.

## 2. Turbulent mixing: The Stommel and Welander models

The purpose of this section is to review the physical basis and results of the Stommel (1961, 1986) and Welander (1982) models of a two-layer system forced by heating and evaporation, and mixed by turbulent diffusion. In the original development of the models, the relation of the model parameters to their dimensional real-world counterparts was not obvious. We discuss the form and magnitude of the forcing and mixing terms, and their relation to the nondimensional parameters. Also, Stommel's (1987)

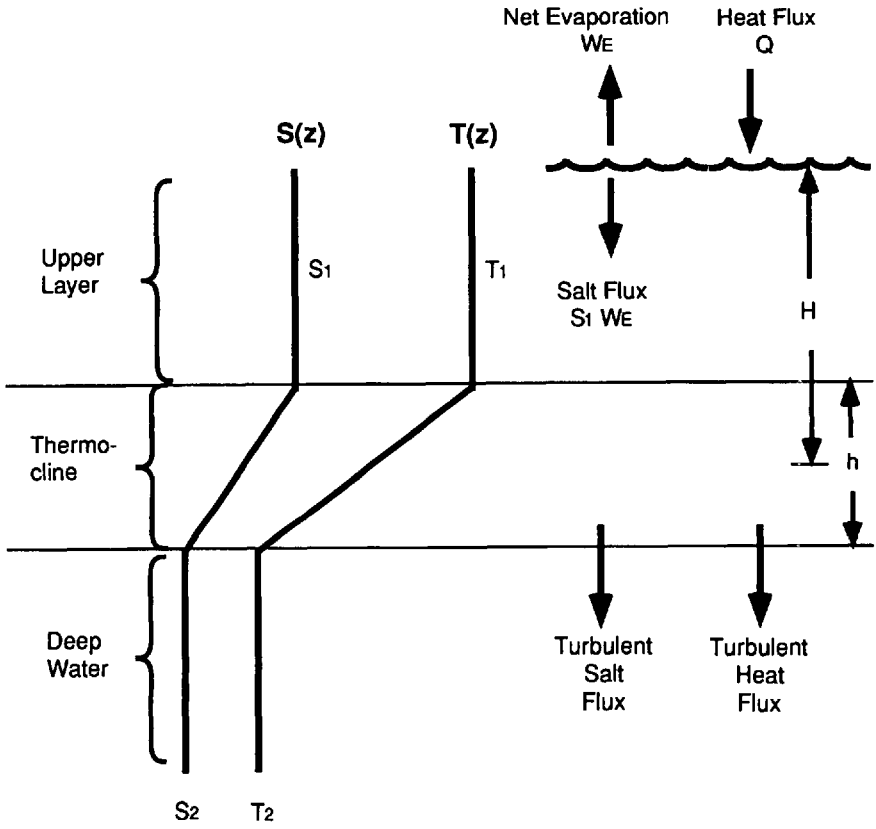


Figure 2. Definition sketch for the Stommel/Welander model. Heating and evaporative salt fluxes at the ocean surface are removed from the upper layer by turbulent mixing through the thermocline, which is assumed to be of constant thickness, $h$.

discussion appeared in Ocean Modeling, which is not generally available, so it seems worthwhile to review these results and give a unified discussion of them.

### *a. The turbulent mixing model*

*(i). Physical basis.* We start by considering the ocean to be effectively one-dimensional, with weak lateral advection and mixing effects. The neglect of lateral effects can be either justified locally in individual cases, or by noting that a vertical balance dominates the picture for a closed gyral system. The vertical stratification of temperature ($T$) and salinity ($S$) is idealized in the manner shown in Figure 2, with an upper layer (subscript 1), a thermocline, and cooler, less saline deep water (subscript 2). The deep water, having large volume, is assumed to have constant properties, and we also neglect time variations in thermocline thickness, $h$, and the depth from the surface to mid-thermocline, $H$. The upper layer is warmed by the net surface heating, $Q$[W m$^{-2}$],

and increased in salinity by the excess evaporation over precipitation, $w_E$ [m s$^{-1}$]. The turbulent salt and heat fluxes through the thermocline tend to cause the upper layer salinity and temperature to decrease. The effects of these fluxes on the deep water, and the cold and freshness carried upward by the slow upwelling of deep water, are ignored in this simple model.

*(ii). Flux parameterizations.* Haney (1971) analyzed the zonally and time averaged net surface heat flux, calculated from the bulk formulae for radiative, sensible, and latent heat flux, and deduced that the net flux was well described by a first-order dependence on ocean surface temperature:

$$Q = B^* \alpha(T_0 - T_1) \tag{2.1}$$

where $T_0$ is an apparent equilibrium temperature, representative of the net thermal forcing from the atmosphere. Haney found $T_0$ to be a strong function of latitude, varying from 31°C at the equator to 4°C at ±45° latitude. $B^*$ is a coefficient found from comparing the averaged flux data with ocean surface temperatures, and was found by Haney to be about 80 ly day$^{-1}$ C$^{-1}$ = 39 W m$^{-2}$ (1 ly d$^{-1}$ = 0.484 W m$^{-2}$), varying only 20% with latitude.

The surface evaporation is parameterized by a bulk formula similar to that for sensible heat flux (see, for example, Haney, 1971, Eq. 17 et seq):

$$\text{Evaporation} = \rho_A C_D V_A[q_1(T_1) - q_A] \tag{2.2}$$

where $\rho_A$ is the air density, $C_D$ a drag coefficient, $V_A$ the wind speed at anemometer level, $q_A$ the specific humidity of the air at anemometer level, and $q_1(T_1)$ the saturation specific humidity at the temperature of the ocean surface $T_1$. Haney wrote the temperature dependence of $q_1$ in a truncated Taylor series, and evaluated the lowest and first order coefficients as a function of latitude. From Haney's Eq. 26:

$$w_E = w_{E0} + w_{E1}(T_A - T_1) \tag{2.3}$$

where $w_E$ is the mean rate of evaporation minus precipitation, $T_A$ is the actual atmospheric temperature, and $w_{E1}$ is the rate of change of evaporation minus precipitation with surface temperature. Assuming $w_{E1}$ is mainly due to a temperature effect on evaporation and not on precipitation, Figure 6 of Haney (1971) shows that $w_{E1} \approx 50$ ly d$^{-1}$ C$^{-1}$/(595 cal gm$^{-1}$) = $9 \times 10^{-9}$ m s$^{-1}$ C$^{-1}$. When this value is compared to a typical value of $w_{E0}$ of 1 m y$^{-1}$ ($3.17 \times 10^{-8}$ m s$^{-1}$ C$^{-1}$) for the subtropical North Atlantic (Schmitt *et al;* 1989), we find that a temperature change of only 3.5 C will change the net evaporation–precipitation by 100%, suggesting that the temperature dependence of evaporation rate is strong. However, the important point here is that $w_E$ does not depend on the salinity of the surface water.

The turbulent transports of salt and heat through the thermocline from the top layer are parameterized by an eddy diffusivity $K$ which is equal for heat and salt:

$$\beta F_S = \frac{K}{h}\beta(S_1 - S_2) \tag{2.4a}$$

$$\alpha F_T = \frac{K}{h}\alpha(T_1 - T_2). \tag{2.4b}$$

The diffusivity is assumed to be a function of the gradient Richardson number (Munk and Anderson, 1948):

$$K = K_0 A(Ri) \tag{2.5}$$

where

$$Ri = -\frac{g}{\rho}\frac{\partial \rho}{\partial z}|v_z|^{-2} \tag{2.6}$$

and $|v_z|$ is the magnitude of the velocity shear. As we expect most of the thermocline mixing to be driven by breaking internal waves, and our main concern here is how the rate of mixing varies with density stratification, we view the shear to be a mean square value, and assume it to be constant for the purposes of this model. The density gradient in 2.6 is taken to be that in the main thermocline, $gh^{-1}[\beta(S_1 - S_2) - \alpha(T_1 - T_2)]$. ($\beta$ and $\alpha$ are the haline and thermal expansion coefficients.) The constant $K_0$ is described by Munk and Anderson (1948) as the value which the eddy diffusivity would take in the absence of stratification; this is a useful concept for turbulence driven by steady shear, but is confusing at best for the case of breaking internal waves. We discuss the functional forms for $A(Ri)$ and their relation to the theory later in Section 2d.

*(iii). Equations and nondimensionalization.* With the above parameterization for fluxes, the equations expressing conservation of salinity and temperature for the upper layer and thermocline are:

$$H\frac{d}{dt}\beta(S_1 - S_2) = w_E\beta S_1 - \frac{K}{h}\beta(S_1 - S_2) \tag{2.7a}$$

$$H\frac{d}{dt}\alpha(T_1 - T_2) = \frac{B^*}{\rho c_p}\alpha(T_0 - T_1) - \frac{K}{h}\alpha(T_1 - T_2). \tag{2.7b}$$

These can be made nondimensional by scaling temperatures by $(T_0 - T_2)$, salinities by $\alpha(T_0 - T_2)/\beta$, and time by the diffusive timescale $Hh/K_0$, to yield:

$$\frac{dS}{dt} = E - AS \equiv P(S, T) \tag{2.8a}$$

$$\frac{dT}{dt} = B(1 - T) - AT \equiv Q(S, T) \tag{2.8b}$$

where

$$S = \beta(S_1 - S_2)/\alpha(T_0 - T_2)$$

$$T = \alpha(T_1 - T_2)/\alpha(T_0 - T_2)$$

$$t = t_{\text{dim}} K_0 (Hh)^{-1}$$

$$B = \frac{B^*}{\rho c_p} \frac{h}{K_0}$$

$$E = E_0 + E_1(1 - T)$$

$$E_0 = w_{E0} \frac{h}{K_0} \left( \frac{\beta S_2}{\alpha(T_0 - T_2)} + S \right)$$

$$\approx w_{E0} \frac{h}{K_0} \frac{\beta S_2}{\alpha(T_0 - T_2)} \qquad \text{(Assuming } S_1 - S_2 \ll S_2\text{)}$$

$$E_1 \approx w_{E1} \frac{h}{K_0} \frac{\beta S_2}{\alpha} \qquad \text{(Assuming } S_1 - S_2 \ll S_2 \text{ and } T_A \approx T_0\text{).}$$

We assume the following values for external parameters in order to estimate timescales and magnitudes of forcing parameters:

$$h = H = 500 \text{ m}$$

$$T_0 - T_2 = 30°\text{C} \qquad \text{(Haney, 1971)}$$

$$K_0 = 10^{-4} \text{ m}^2\text{s}^{-1}$$

$$B^* = 39 \text{ W m}^{-2}(°\text{C})^{-1} \qquad \text{(from Haney, 1971 discussed above)}$$

$$w_{E0} = 3 \times 10^{-8} \text{ m s}^{-1} \qquad \text{(Schmitt } \textit{et al.}\text{, 1989)}$$

$$w_{E1} = 9 \times 10^{-9} \text{ m s}^{-1}(°\text{C})^{-1} \qquad \text{(From Haney, 1971 discussed above)}$$

$$\alpha = 2 \times 10^{-4}(°\text{C})^{-1}.$$

With these values, the timescale $hH/K_0 \approx 300$ days. Typical values for the forcing parameters are:

$$B = 45$$

$$E_0 = 0.74$$

$$E_1 = 6.7.$$

The fact that $B$ greatly exceeds $E$ suggests that the ocean surface temperature responds relatively quickly to changes in atmospheric temperature.

In terms of dimensionless variables, the gradient Richardson number becomes

$$Ri = \frac{g\,\alpha(T_0 - T_2)}{|v_z|^2\, h}(T - S) = \frac{T - S}{\Delta\rho} = -\frac{\rho}{\Delta\rho} \tag{2.9}$$

Note that $\rho = S - T$ is the nondimensional density difference between the layers. Munk (1981) argued that the internal wave field is in a state of incipient breaking ($Ri$ near $1/4$), so that $|v_z|^2 \approx 4N_0^2$, where $N_0 \approx 3$ cph, the scaling value for the main thermocline buoyancy frequency in the GM 79 internal wave spectrum (Munk, 1981). With the scale values above, we find $\Delta\rho \approx 1$, with a factor of several uncertainty. Note that $\Delta\rho$ is a dimensionless quantity which determines the width of the zone of strong variation in mixing on the $T$-$S$ phase plane, the region of the plane in which the Richardson number is order one.

*b. Stommel's models*

Stommel (1961) investigated an exceptionally simple model of convection which consisted of two equal volume reservoirs connected by exchange pipes. His model can be envisaged as two old-style radiators, one heated and one cooled, connected by pipes top and bottom in such a way that gravity acting on the density difference of the water causes horizontal exchange. Increasing density difference caused increased exchange. Steady heating and cooling would then cause a flow of water from the warm radiator to the cold one via the upper pipe, and a return flow via the lower pipe, in much the same manner as a gravity-fed hot-water heating system. Stommel then imagined that the reservoirs were forced by salt fluxes, acting in opposition to the heating fluxes. The warm radiator suffered a net evaporation, and the cooler one a net precipitation. Stommel then found that there were three steady states, one of which was unstable. One stable steady state corresponded to the heat-driven circulation described above, while the other stable steady state was dominated and driven by the salt flux, and flowed in the opposite direction. Which state occurred in any situation depended on the precise initial conditions.

Stommel (1986) envisioned the reservoirs to be connected vertically, in imitation of a two-layer vertically mixed system. In this case the rate of exchange, representing the vertical turbulent mixing, increased as the density difference became closer to zero. This corresponds to the situation discussed in Section 2a, (Eq. 2.8), in which $A(Ri)$ is a decreasing function of $Ri$. Stommel (1986) took the evaporation rate $E$ to be constant, and showed analytically that when $A$ was a step function, decreasing abruptly when a critical density difference (say $|\rho| \approx 0.1$ for the purpose of this discussion) is exceeded, the system will cycle. He showed that the steady state corresponding to $|\rho| > 0.1$ lay in the $|\rho| < 0.1$ region, and vice-versa, so that the system was forever searching for steady state and not finding it. (This description is quite reminiscent of the use of the

Poincare-Bendixson theorem used in the next section.) Stommel (1986) then demonstrated the limit cycle numerically for a Gaussian function with continuous dependence of $A$ on $\rho$.

The physical description of the cycle is very simple: if we imagine the system starting with $\rho > 0.1$, then mixing can be ignored initially. The upper layer becomes warmer (and lighter), until $T$ becomes close to the atmospheric equillibrium value and warming slows down. Evaporation continues, however, and causes the upper layer to become more saline and more dense. As $S$ increases, the density difference between the top and bottom layers will decrease, and eventually be small enough to allow the rate of mixing to increase suddenly. Mixing can then dominate in this stage of the cycle, and cause the $T$ and $S$ to both decrease. The heating then becomes important, and warms the water to the point where mixing again becomes unimportant and the cycle begins anew. Thus the cycle involves the dominance, in turn, of heating, then evaporation, then mixing.

### *c. Welander's model*

Stommel (1986) (and we) were unaware of the model described by Welander (1982), which is quite similar to Stommel's. Welander (1982) started with a system of two vertically-separated layers represented by the dimensionless equations:

$$\frac{dS}{dt} = \kappa_S(S_A - S) - AS \tag{2.10a}$$

$$\frac{dT}{dt} = B(1 - T) - AT. \tag{2.10b}$$

The dependence of the salinity forcing on $S$ rather than $T$ does not seem to be very physical, but this difference does not profoundly affect the model results. Also, if Welander's $\kappa_S$ is allowed to approach zero, and his $S_A$ to approach infinity in such a way that the product $\kappa_S S_A = E$ is constant, then Stommel's model (2.8) is recovered. Welander's analysis of the system is fairly detailed, and his analysis of the conditions under which oscillations may occur is quite illuminating in terms of the physical mechanism, and useful for comparison with the similar results for salt fingers. We rederive some of his results here, in our notation. In the remainder of this paper, we make use of several theorems used for qualitative analysis of two-variable autonomous nonlinear systems. The concept of the phase plane, critical points, and those theorems are introduced in the Appendix.

First, we set $P = Q = 0$ in (2.8) to find the equilibrium (denoted by overbar) points $\overline{S}=E/A$, and $\overline{T}=B/(A+B)$, which may be found from the transcendental equation

$$\overline{\rho} = \overline{S} - \overline{T} = \frac{-B}{A + B} + \frac{E}{A}. \tag{2.11}$$

For constant $E$, (2.11) may be solved graphically by plotting the right-hand side as a function of $\rho$, and looking for the intersection with a line of slope 1, representing $\overline{\rho}=\rho$. This is demonstrated by both Stommel (1961) and Welander (1982). For $E \neq$ constant, the equilibrium points may be found by computer iteration. For specific forms of $A(\rho)$ in which $A$ decreases for increasing $|\rho|$, a single equilibrium point may be found. Perturbations from this point are determined by a linear $2 \times 2$ system with eigenvalues given by the equation:

$$\lambda^2 - F\lambda + G = 0 \tag{2.12}$$

where

$$F(\overline{S}, \overline{T}) = \left(\frac{\partial P}{\partial S} + \frac{\partial Q}{\partial T}\right)_{\text{equil}}$$

$$= -(B + 2A(\overline{\rho}) + \overline{\rho}A') \quad (\text{Here, } A' = \partial A/\partial\rho|_{\text{equil}}). \tag{2.13}$$

$$G(\overline{S}, \overline{T}) = \left(\frac{\partial P}{\partial S}\frac{\partial Q}{\partial T} - \frac{\partial P}{\partial T}\frac{\partial Q}{\partial S}\right)_{\text{equil}}$$

$$= A(B + A) + A'\left\{\frac{-AB}{A + B} + E\left(1 + \frac{B}{A}\right) + \frac{B}{A + B}\left(\frac{\partial E}{\partial T}\right)_{\text{equil}}\right\}. \tag{2.14}$$

Now, $\lambda$ will have a positive real part, signifying unstable growth, when $F > 0$. Since all trajectories "point in" at the boundary, so that all initial conditions starting at a boundary point evolve to the interior, we can apply the Poincare-Bendixson theorem (see Appendix). This states that if all trajectories enter the phase plane from the boundary, and the only critical point is unstable so trajectories cannot lead there, then there must be a limit cycle which all trajectories approach. Therefore $F(\overline{S}, \overline{T}) > 0$ implies the existence of a limit cycle. Poincare's index theorem then shows that the limit cycle must enclose the critical point, which must be an unstable node or spiral. After deriving the above result, Welander proceeded to demonstrate the cycle numerically for a particular form of $A(\rho)$.

Note that the dependence of evaporation rate $E(T)$ on temperature does not affect $F$, and so does not directly affect the existence of a limit cycle.

*d. Richardson number effects on mixing rate*

From Eq. 2.13, a necessary condition for a limit cycle is for the term $\overline{\rho}A'$ to be large and negative. This requires a large positive value of $A'$ at a finite negative value of $\overline{\rho}$, corresponding to an abrupt increase in mixing rate at small *but finite* gravitational stability. The Gaussian chosen by Stommel (1986) and the trignometric form chosen by Welander (1982) have this property, but neither form has been suggested or adopted as a suitable parameterization for stratified turbulence.

Gargett (1984) examines evidence from tracer observations and re-capitulates the thesis of Gargett and Holloway (1984) to conclude that the diffusivity associated with

breaking internal gravity waves may vary with $N$, the buoyancy frequency (where $N^2 = -(g/\rho)\,\partial\rho/\partial z$) such that $K = cN^{-m}$, where $c$ is a constant and $m \approx +1$. This translates to $A = c|\rho|^{-n}$, where $n = m/2$. This has a singularity at $\rho = 0$, with infinite slope on either side, and so would seem to offer some likelihood of satisfying 2.13 and allowing a limit cycle in the model. However, performing the differentiation, we find that $|\rho A'| = nA$, and so in 2.13, $F(\bar{S}, \bar{T}) = -[B + (2 - n)\,A(\bar{\rho})]$. Therefore $F$ cannot be greater than zero unless $n > 2$ (i.e., $m > 4$). This is well outside the range of uncertainty found by Gargett (1984). The reason why this function fails to satisfy 2.13 even though $A'$ is infinite is because the infinite slope occurs at $\rho = 0$, whereas a large slope at finite $\rho$ is needed. The formulations commonly used for shear-driven stratified turbulence, described in the next paragraph, have this property.

Munk and Anderson (1948) proposed the form

$$K = K_0(1 + c\,Ri)^{-n} \tag{2.15}$$

for the diffusivity of heat in stratified turbulence. This corresponds to the dimensionless form:

$$A = \left(1 + \frac{c(T - S)}{\Delta\rho}\right)^{-n}. \tag{2.16}$$

Henderson-Sellers (1982) reviews the range of values suggested for $c$ and $n$, with most authors taking $n$ to be in the range ($\frac{1}{2} - \frac{3}{2}$). Pacanowski and Philander (1981) used 2.15 in modelling the tropical thermocline, and selected $n = 2.5$.

Henderson-Sellers (1982) reviewed several parameterizations for momentum and mass diffusivities, and compared them with observational data. He suggested that the observations are well fit by:

$$A(Ri) = (1 + 37\,Ri^n)^{-1} = \left(1 + 37\left(\frac{T - S}{\Delta\rho}\right)^n\right)^{-1} \tag{2.17}$$

with $n = 2$.

Both 2.16 and 2.17 have the desired property of a rapid change of $A$ and a finite value of $\rho$. Is the slope steep enough to allow a limit cycle? By differentiating 2.16 (with $\rho = T - S$) we find:

$$A' = n\left(\frac{c/\Delta\rho}{1 - c\rho/\Delta\rho}\right)\frac{A}{\rho} \tag{2.18}$$

so that $|A'\rho| \leq \frac{1}{2}n\,(2A)$, and so 2.13 can not be satisfied unless $n > 2$. Similarly, by differentiating 2.17, we find:

$$A' = -n\left(\frac{37(\rho/\Delta\rho)^n}{1 + 37\,(\rho/\Delta\rho)^n}\right)\frac{A}{\rho} \tag{2.19}$$

and again 2.13 cannot be satisfied unless $n > 2$.

Of the forms for $A(Ri)$ discussed above, only that by Pacanowski and Philander (1981) is sufficiently steep at finite $Ri$ to allow the possibility of oscillation in the two-layer system represented by 2.8. Even that form, 2.16 with $n = 2.5$, is only marginally steep enough to allow cycling. Peters *et al.* (1988) observed systematic variation of measured eddy coefficients with $Ri$ in the Equatorial Pacific. After much averaging, they found 2.16 to be roughly appropriate at high $Ri$, and they observed a very abrupt increase in eddy diffusivity at low $Ri$, in the range $\frac{1}{4} < Ri < \frac{1}{2}$. This increase was so steep it corresponded to $A \propto (Ri)^{-(10\pm4)}$ which would certainly be steep enough to allow oscillation in the model. However, the equatorial undercurrent is very special in that the shear which drives turbulent mixing is strong and steady, whereas mixing in the main thermocline away from the equator is likely to be highly intermittent. Mixing by occasional breaking internal waves has the effect of averaging over many events with different intensities. This should have the effect of smoothing the dependence of eddy diffusivity on average $Ri$ (or alternatively, internal wave field inverse Froude number), and may be the factor responsible for the relatively weak variation of eddy diffusivity with buoyancy frequency found by Gargett (1984). Thus, the sharp dependence of $A$ on $Ri$ found by Peters *et al.* (1988) may not occur in regions mixed by breaking internal waves. Although the appropriate parameterization of eddy diffusivity associated with breaking internal waves is still very much an open question, it appears so far as though the dependence on static stability is too gradual to permit limit oscillations to occur.

Note that, for oscillations to occur in the system 2.8, the upper layer is warmer and saltier than the lower, and the salinity and temperature differences tend to be comparable in density terms. In other words, the density ratio, $R_\rho = S/T$, tends to be $O(1 - 2)$. (The example shown by Welander had $R_\rho \approx 1.07$.) Schmitt (1981) argues that salt finger mixing is likely to dominate turbulent mixing when the density ratio is much less than 2, so we might expect the system described here to be mixed by salt fingers rather than mechanical turbulence. In the next section we explore the effect of salt finger mixing on the system.

## 3. Mixing by salt fingers—The "4/3 law" parameterization

Denote the temperature and salinity of the upper and lower layers in Figure 1 by $T_1$, $S_1$, $T_2$, $S_2$. Assuming the lower layer is much thicker than the upper, and so neglecting the changes of the lower layer, the *dimensional* conservation equations for the upper layer are:

$$H\frac{d}{dt}\beta(S_1 - S_2) = w_E\beta S_1 - \beta F_S \tag{3.1a}$$

$$H\frac{d}{dt}\alpha(T_1 - T_2) = \frac{B^*}{\rho c_p}\alpha(T_0 - T_1) - \alpha F_T. \tag{3.1b}$$

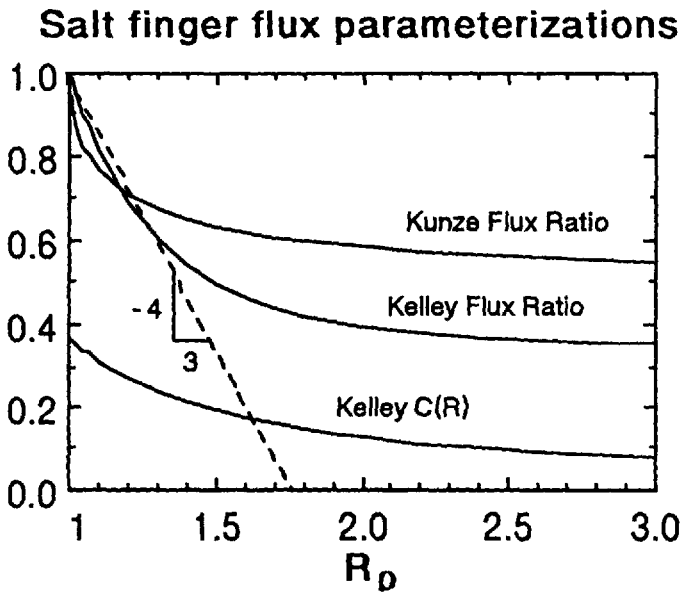


Figure 3. Parameterization of the flux coefficients used in (3.2): $C(R_\rho) = 0.04 + 0.327\, R_\rho^{-1.9)}$, and $\gamma(R_\rho) = 0.35 \exp\{1.05 \exp[-2.16(R_\rho - 1)]\}$, both from Kelley (1986), and $\gamma(R\rho) = (R_\rho^{1/2} - (R_\rho - 1)^{1/2})R_\rho^{1/2}$ (Kunze, 1987). The Kunze parameterization for $\gamma$ is obtained from local instability theory for the fastest growing fingers, while Kelley's $C$ and $\gamma$ are fits to available laboratory measurements. The two formulations for $\gamma$ appear to be upper and lower bounds for the observed flux ratio in the range $1 < R_\rho < 3$.

We parameterize the fluxes $F_S$ and $F_T$ in a manner appropriate to salt finger mixing across a sharp interface, using the "4/3 power laws," which can be deduced by dimensional analysis (Turner, 1973):

$$\beta F_S = (g\kappa_T)^{1/3}\, C(R_\rho)\, (\beta(S_1 - S_2))^{4/3} \tag{3.2a}$$

$$\alpha F_T = \gamma(R_\rho)\beta F_S \tag{3.2b}$$

where the density ratio $R_\rho = \alpha(T_1 - T_2)/\beta(S_1 - S_2)$ must be greater than 1 for the upper layer to be less dense than the lower. The flux ratio, $\gamma$, must be less than 1 in the absence of external sources of potential energy; this ensures an upward buoyancy flux, and a release of potential energy which drives the convection. This, and the dependence on $R_\rho$ is the major difference between double-diffusive mixing and mechanical mixing, which results in a downward buoyancy flux.

Laboratory experiments have established unequivocally that both $\gamma(R_\rho)$ and $C(R_\rho)$ are nonincreasing functions of $R_\rho$. Early work (described in Turner, 1973) found $\gamma$ to be approximately constant at 0.56, and later laboratory studies (reviewed in Kunze, 1987) found $\gamma$ to systematically decrease with increasing $R_\rho$. Typical "4/3 flux law" parameterizations for salt finger transport coefficients are shown in Figure 3, from Kelley (1986) and Kunze (1987).

The nondimensional form of (3.1) with the parameterization (3.2) is:

$$\frac{dS}{dt} = E - C(R_\rho)\, S^{4/3} = P(S, T) \tag{3.3a}$$

$$\frac{dT}{dt} = B(1 - T) - \gamma(R_\rho)\, C(R_\rho)\, S^{4/3} = Q(S, T) \tag{3.3b}$$

where

$$S = \beta(S_1 - S_2)/\alpha(T_0 - T_2)$$
$$T = \alpha(T_1 - T_2)/\alpha(T_0 - T_2)$$
$$t = t_{\text{dim}}[g\kappa_T\alpha(T_0 - T_2)]^{1/3}/H$$
$$B = \frac{B^*}{\rho c_p}\,[g\kappa_T\alpha(T_0 - T_2)]^{-1/3}$$
$$E = w_E\beta S_2(g\kappa_T)^{-1/3}\,[\alpha(T_0 - T_2)]^{-4/3} \qquad \text{(Assuming } S_1 - S_2 \ll S_2\text{)}$$
$$R\rho = T/S.$$

The dimensional time scale, that corresponding to the time taken for the finger fluxes to decrease the salinity, is only 3 days using the values from Section 2 for $H$, etc. The magnitude of $C(0)$, about 0.1 for heat-salt fingers, could have been included in the scaling for time. This would increase the time scale to 30 days. However, we chose to include it explicitly in the dimensionless equations. In a salt finger model using flux/gradient parameterizations, Schmitt (1981) found time-scales of several months to a few years to be appropriate when realistic thermocline and upper layer thicknesses were used. The reason the time-scale is so much shorter in this model is because we have used a formulation appropriate for a single interface, rather than gradients or many smaller interfacial steps. Similarly, when realistic forcing values $B^*$ and $w_E$ are substituted from Section 2, we find the computed $E$ and $B$ to both be very much smaller than 1. This is because the equations are trying to tell us that the observed rate of atmospheric forcing would be small compared to the mixing across a single sharp salt fingering interface bounded by a 500 m deep convecting layer. If we imagine the thermocline region to consist of a sequence of interfaces, each with a much smaller salinity and temperature difference acting across it, then the model equations would be similar in form to 3.3, but with a more realistic time scale and with larger $E$ and $B$. The computed examples shown later are run for larger $E$ and $B$, since small $E$ and $B$ result in virtually linear equations.

We now consider the behavior of (3.3), by considering the equilibrium points of the system, and then looking for conditions under which a cycle can occur. Steady solutions occur for

$$\overline{S} = (E/C)^{3/4} \tag{3.4a}$$

$$\overline{T} = 1 - \gamma E/B. \tag{3.4b}$$

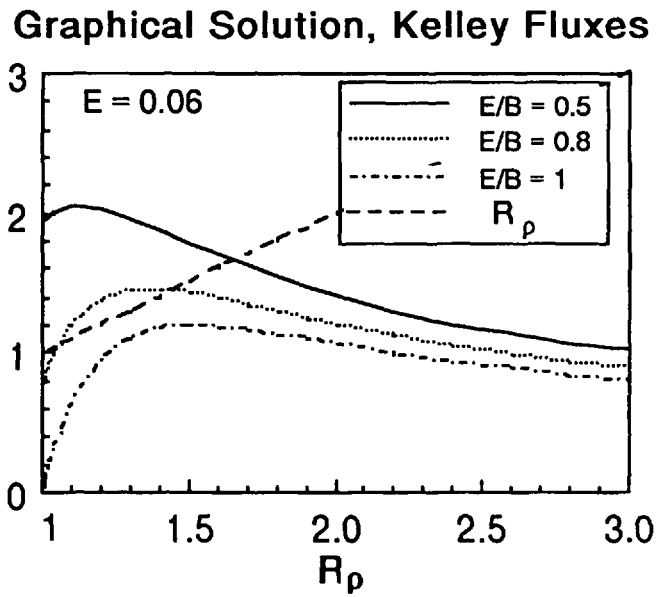


Figure 4. Graphical solution of (3.5) for three values of $B$, and for $E = 0.06$, showing one, two, and zero equilibrium points respectively.

Taking the ratio of (3.4a) and (3.4b) gives a transcendental equation for $R_\rho$:

$$R_\rho = [C(R_\rho)/E]^{3/4}(1 - \gamma(R_\rho)\, E/B). \tag{3.5}$$

We will first consider the case of constant flux ratio, and then the more general case.

*a. Constant flux ratio*

The left side of (3.5) is an increasing function of $R_\rho$, with slope 1. If $\gamma$ = constant, then the right side of (3.5) is a decreasing function of $R_\rho$, due to the fact that $C(R_\rho)$ is a decreasing function. Thus, for constant flux ratio, there is at most one equilibrium point, given by the intersection of the two curves. It is a simple matter to plot the left and right sides of 3.5 in order to solve it graphically, in the manner demonstrated in Figure 4 for nonconstant flux ratio.

By Bendixson's first theorem (see Appendix), a necessary condition for the existence of a limit cycle is that

$$F(S, T) = \left(\frac{\partial P}{\partial S} + \frac{\partial Q}{\partial T}\right) = -B + S^{1/3}[(R_\rho - \gamma)C' - (4/3 + \gamma')C] \tag{3.6}$$

must change sign within the cyclic trajectory. (Here, $\gamma' = \partial\gamma/\partial R_\rho$, and $C' = \partial C/\partial R_\rho$. We allow nonconstant $\gamma$ here so that 3.6 can be used in the next section.) Now, the first two terms are negative, and for constant flux ratio or even if $\gamma' > (-4/3)$, so is the third. Thus, if the flux ratio is either constant or varies weakly, (3.6) is always negative, and no limit cycle is possible.

There are situations for which no equilibrium point occurs, when $(1 - \gamma E/B)^{4/3}$ $(C(1)/E) < 1$. This corresponds to the evaporation being too strong for the salt finger fluxes to keep up. In these situations the maximum value of the right-hand side of (3.5) at $R_\rho = 1$ is less than 1. We would intuitively expect the upper layer to become more dense than the lower, and overturn. Checking the rate of change of density at the boundary $R_\rho = 1$ gives:

$$\left.\frac{d(S-T)}{dt}\right|_{T=S=1-\gamma E/B} = E(1-\gamma)\,(1-(1-\gamma E/B)^{4/3}\,(C(1)/E)) > 0. \quad (3.7)$$

Therefore there is a section around $T = S = (1 - \gamma E/B)$ which has $d\rho/dt > 0$, causing the upper layer to become denser than the lower, and to overturn. There is no equilibrium point in this situation, so all initial conditions will overturn, passing through this section.

So, for constant flux ratio, there is at most one equilibrium point; if it exists, then it is a stable node or spiral. If the point does not exist, then all initial conditions will lead to overturning.

*b. Variable flux ratio*

We note that (3.6) can change sign if $\gamma' < (-4/3)$, and both the Kelley and Kunze parameterizations have sufficiently rapid variation of the flux ratio for $R_\rho \leq 1.1$ for this to occur. Thus, it appears at first glance as though a limit cycle may be possible if the flux ratio varies sufficiently rapidly. This is reminiscent of Huppert's (1972) result that a series of double-diffusive layers has a stable equilibrium if and only if the flux ratio is constant. However, we see in this section that even if $\gamma' < (-4/3)$, the system will not cycle.

If $\gamma$ decreases with increasing $R_\rho$, then the right side of (3.5) is a decreasing function at large $R_\rho$ as before, but at small $R_\rho$, it can be an increasing function, due to the variation of $\gamma$. This behavior is illustrated in Figure 4, in which (3.5) is solved graphically. It can be seen that for some values of $E$ and $B$, there are two equilibrium solutions, the one at large $R_\rho$ corresponding to the $\gamma$ = constant solution, and one at smaller $R_\rho$ which exists only because of the variation of the flux ratio. A third equilibrium solution corresponding to negative $(1 - \gamma E/B)$ exists, but corresponds to negative $T$, and so is not physical.

In the remainder of this section, we show that the equilibrium point at low $R_\rho$ is a saddle, and that the one at higher $R_\rho$ is a stable node or spiral. We then use Poincare's Index theorem (see the Appendix) to argue that if a limit cycle exists, it must encircle the node/spiral, but not the saddle. We then find that because the node/spiral is a stable one, then by Bendixson's theorem, there can be no limit cycle.

Perturbations from either of the two equilibrium points are determined by a $2 \times 2$ system with eigenvalues given by the equation:

$$\lambda^2 - F\lambda + G = 0 \quad (3.8)$$

where

$$F(\bar{S}, \bar{T}) = \left(\frac{\partial P}{\partial S} + \frac{\partial Q}{\partial T}\right)_{\text{equil}}$$
$$= (-B + S^{1/3}[(R_\rho - \gamma)C' - (4/3 + \gamma')C])_{\text{equil}}$$
$$G = \left(\frac{\partial P}{\partial S}\frac{\partial Q}{\partial T} - \frac{\partial P}{\partial T}\frac{\partial Q}{\partial S}\right)_{\text{equil}}$$
$$= \left(S^{1/3}\left(\frac{4}{3}BC + \frac{4}{3}S^{1/3}C^2\gamma' - R_\rho BC'\right)\right)_{\text{equil}}$$

and using (3.4) and (3.5), we find

$$G = \left(S^{1/3}C\left(\frac{4}{3}B + \frac{4}{3}S^{1/3}C\gamma' - \left(\frac{B}{E} - \gamma\right)C'S^{1/3}\right)\right)_{\text{equil}}. \tag{3.9}$$

If $G$ is negative, then the quadratic equation (3.8) has two real roots, one positive and one negative, and the equilibrium point is a saddle. If $G$ is positive, then the equilibrium point is a node if $0 < G < F^2/4$ (two real roots of the same sign), or a spiral if $G > F^2/4$ (complex roots). For either a node or spiral, the real part of the eigenvalues is positive (unstable) or negative (stable) according as $F > 0$ or $F < 0$ respectively.

Now, the left and right intersections on Figure 4, occur with the slope of the rhs of (3.5) greater and less than 1 respectively. For both equilibrium points we have:

$$\frac{d}{dR_\rho}\left(\left(1 - \gamma\frac{E}{B}\right)\left(\frac{C}{E}\right)^{3/4}\right)_{\text{equil}} = B^{-1}\left(-\gamma' C\left(\frac{E}{C}\right)^{1/4} + \frac{3}{4}\left(\frac{B}{E} - \gamma\right)C'\left(\frac{E}{C}\right)^{1/4}\right)_{\text{equil}}$$
$$= B^{-1}\left(-\gamma' C S^{1/3} + \frac{3}{4}\left(\frac{B}{E} - \gamma\right)C'S^{1/3}\right)_{\text{equil}} = 1 - G\left(\frac{4}{3}BS^{1/3}C\right)^{-1}_{\text{equil}}. \tag{3.10}$$

Consider the equilibrium point at low $R_\rho$, at which the slope (3.10) of the intersection is greater than 1. Using (3.10), we see that $G < 0$. Therefore, the equilibrium point at low $R_\rho$ is a saddle. Similarly, for the intersection at high $R_\rho$, the slope is less than 1, so $G > 0$, and the equilibrium point at high $R_\rho$ is a node or spiral. Using the fact that the slope in (3.10) is less than 1 for this equilibrium point, and using (3.4):

$$F(\bar{S}, \bar{T}) + \left(\frac{4}{3}CS^{1/3} - C'S^{1/3}\left[R_\rho - \gamma - \frac{3B}{4E} + \frac{3}{4}\gamma\right]\right)_{\text{equil}} < 0. \tag{3.11}$$

If $B/E$ is greater than 1, there is only one equilibrium point and that point corresponds to the one for constant $\gamma$, and is a stable node or spiral. For $B/E < 1$, the term in square brackets is positive, and since $C' < 0$, then (3.11) reads $F$ + (positive terms) $< 0$. Therefore, $F < 0$ for the equilibrium point at larger $R_\rho$, and it is a stable node or spiral.

Poincare's index theorem states that a closed trajectory must enclose an odd number of equilibrium points, and the number of nodes or spirals enclosed must exceed by 1 the

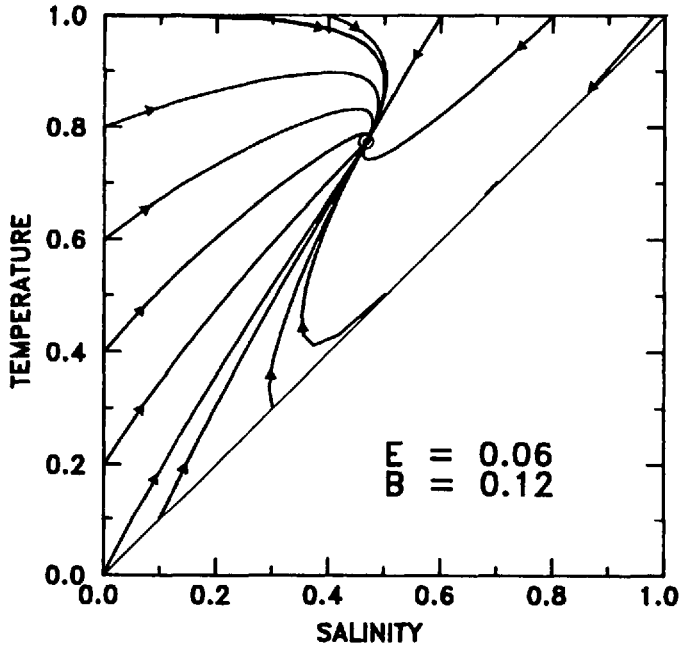


Figure 5. Solutions of (3.3) on the $T$-$S$ phase plane for the situation in Figure 4 with one equilibrium point, a stable node at $(\overline{S}, \overline{T}) = (0.45, 0.77)$.

number of saddles enclosed. In the case at hand, there is a stable node or spiral, and (for variable flux ratio) a saddle. Therefore if a cycle exists, it must enclose only the stable node or spiral, and not enclose the saddle. Clearly the only possibility for a cycle to exist is for the trajectory to surround the node or spiral, and for that node or spiral to be unstable ($F > 0$). However, that equilibrium point was shown to be stable, so no cycle can exist.

*c. Examples of solutions*

Solutions of (3.3) are shown in Figures 5–7 for the three sets of parameter values discussed in Figure 4. The solutions are graphed as $T$ vs. $S$ curves on the $T$-$S$ phase plane. It is helpful to first consider the behavior at the boundaries of the phase plane. On the $T$-axis, where $S = 0$, the only changes are due to evaporation and heating, so the tendency is inward and upward as shown. On the top boundary, where $T = 1$, only evaporation and mixing occur, so the tendency is downward, and can be to the left or the right, depending on the balance between evaporation and mixing. The third boundary corresponds to $R_\rho = 1$, $\rho = 0$. Evaporation, heating, and mixing all occur here, but since $\gamma(1) = 1$, the salt finger buoyancy flux is zero. The difference of (3.3 a,b) gives

$$\left.\frac{d\rho}{dt}\right|_{R\rho=1} = \left.\frac{d(S-T)}{dt}\right|_{T=S} = E - B(1-T). \tag{3.12}$$

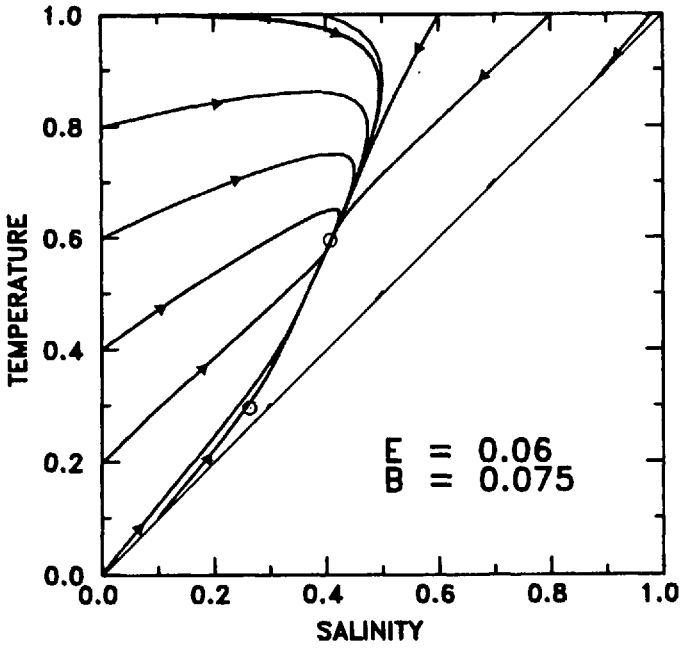


Figure 6. Solutions of (3.3) on the $T$-$S$ phase plane for the situation in Figure 4 with two equilibrium points, a stable node at $(\bar{S}, \bar{T}) = (0.42, 0.6)$, and a saddle at $(\bar{S}, \bar{T}) = (0.27, 0.3)$.

Thus, for $T < -E/B$, $R_\rho = 1$, density decreases, so trajectories point inward, while the reverse is true for $T > 1 - E/B$.

The first case (Fig. 5) is the case with a single equilibrium point, which is a stable node at $R_\rho \approx 1.7$, $\bar{T} \approx 0.77$. Therefore we see that initial conditions sufficiently close to $\rho = 0$ at large $T$ can lead to overturning, but that most initial conditions lead to the stable node. The phase plane for constant flux ratio looks nearly identical to Figure 5, except that the narrow overturning region near $\rho = 1$ is smaller.

As $B$ decreases (refer back to Fig. 4), the stable node moves toward lower $T$, $S$, and $R_\rho$, and as $B$ becomes less than $E/(1 - (E/C(1))^{3/4})$, the second equilibrium point, a saddle, appears at $R_\rho = 1$. For the parameter values shown in Figure 6, the saddle is at $R_\rho \approx 1.1$, $T \approx 0.3$, and its effect on the curvature of nearby trajectories can be seen. The unstable part of the $R_\rho = 1$ boundary has extended to $T = 0.2$, but otherwise the phase portrait is similar to Figure 5.

As $B$ decreases further, the node and saddle merge to a single equilibrium point, at which the slope of the function in Figure 4 (given by 3.10) is equal to 1. Therefore, by (3.10) $G = 0$ at this equilibrium point, so one or more of the eigenvalues is zero, and second order perturbations from equilibrium must be considered. For $B$ smaller than this, there are no equilibrium points, and so by Poincare's index theorem, no cycle can exist. If neither steady states nor cycles can occur, all initial conditions must lead to overturning, and this is what we see in Figure 7. For the case shown, the entire $R_\rho = 1$

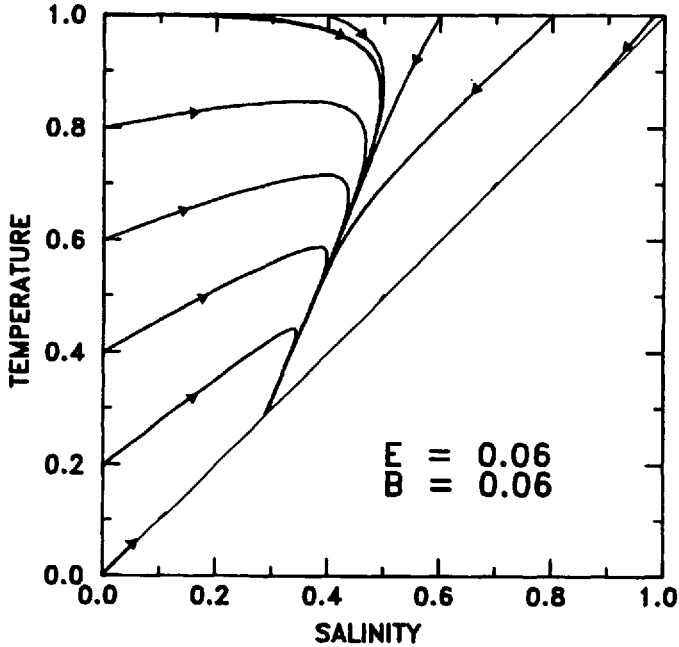


Figure 7. Solutions of (3.3) on the $T$-$S$ phase plane for the situation in Figure 4 with no equilibrium points.

boundary allows overturning, although for some choices of $E$ and $B$, part of the boundary deflects trajectories inward, so that all initial conditions must overturn through the part of the $R_\rho = 1$ boundary with $T > 1 - E/B$. Note that for all finite values of $E$ and $B$, there is some portion of the boundary which allows overturning, so that absolute stability can never be proved.

For the purpose of graphically searching for equilibrium points, (3.5) can be rearranged to give:

$$R_\rho \left( \frac{E}{C(R_\rho)} \right)^{3/4} = \left( 1 - \gamma(R_\rho) \frac{E}{B} \right) (= \overline{T}). \tag{3.13}$$

In Figure 8 the left side of (3.13) is plotted as the solid curves for several values of $E$, and the right side is plotted as the dashed curves for several values of $E/B$, using the Kelley (1986) flux parameterizations. Each intersection of a dashed and solid line represents a possible equilibrium point, and the values of $R_\rho$ and $\overline{T}$ may be obtained directly from the graph. Figure 9 shows the same curves for Kunze's (1987) parameterization of the flux ratio; comparing the two figures shows that the nature of the solutions does not depend strongly on the exact parameterization used.

An example of parameter values which allow a single stable spiral equilibrium point is shown in Figure 10. The values chosen have the equilibrium point (0.775, 0.796), or

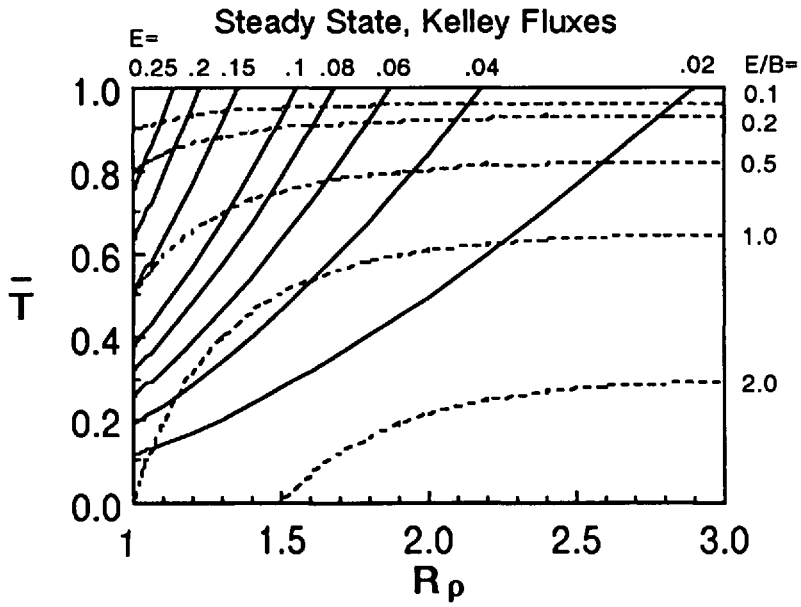


Figure 8. Graphical solution of (3.13) for the flux coefficient parameterization given by Kelley (1986).

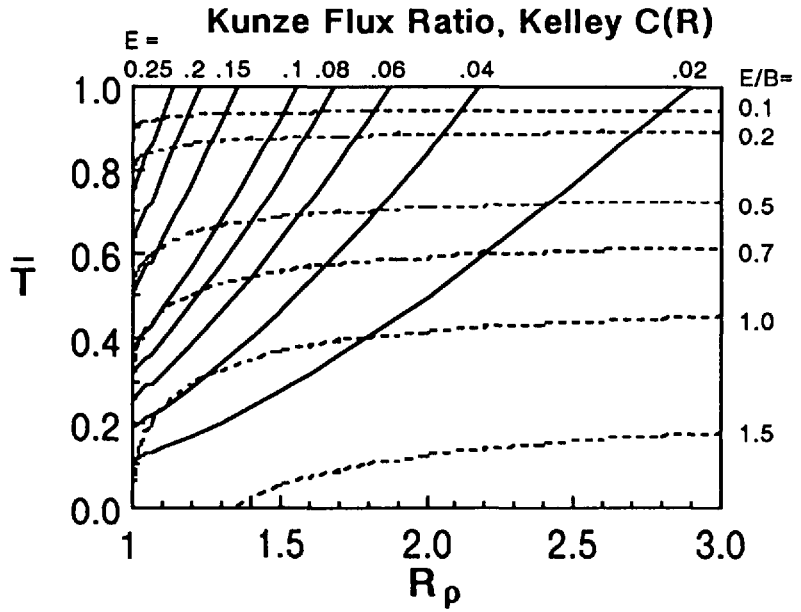


Figure 9. Graphical solution of (3.13) for the Kelley (1986) parameterization of $C$, and the Kunze parameterization of $\gamma$.

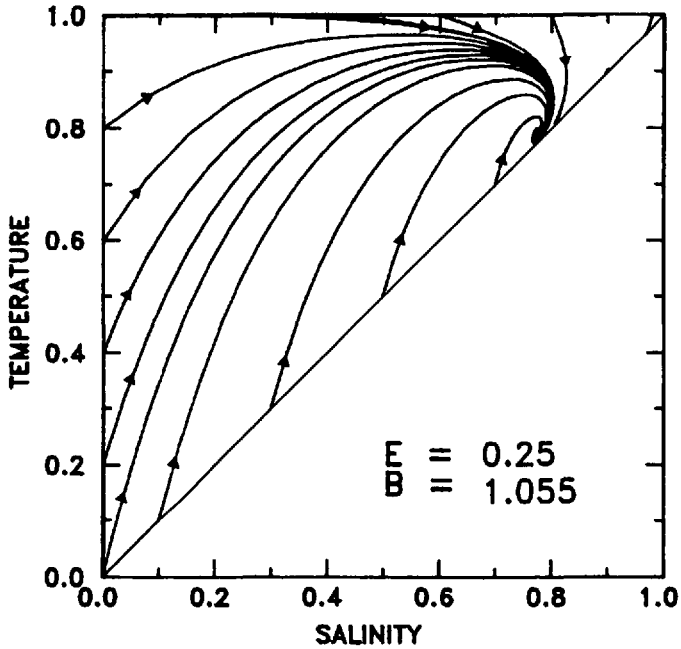


Figure 10. Solutions of (3.3) on the $T$- $S$ phase plane for a situation with a single stable spiral equilibrium point at $(\overline{S}, \overline{T} = (0.78, 0.79)$. Kelley flux parameterization.

$R_\rho = 1.026$. Decreasing $B$ from 1.055 to 1.050, a change of 0.5%, moves this point to $\rho > 0$ and causes all initial conditions to overturn.

When $\rho$ increases above zero, the water column is statically unstable, so that convective mixing occurs throughout the water column, and the upper layer rapidly moves toward (0, 0). Thereafter, the system evolves as predicted by (3.3), i.e., for parameter values as in Figures 5, 6, and 10, steady state is achieved. For $E/B \geq 1$ as in Figure 7, the system is continually overturning since the entire boundary is unstable, and so it can never leave (0, 0).

There is a range of values with $E \leq B$, but with no equilibrium solution, for which a limit cycle exists, involving periodic overturning. Figure 11 is an example. Any initial conditions lead to overturn, and subsequent mixing, so that $T$ and $S$ approach (0, 0). The upper layer then becomes warmer and more saline, along the trajectory leading from (0, 0), and then salt finger mixing becomes stronger, followed by overturn, after which the cycle is repeated.

## 4. Mixing by salt fingers: Flux-gradient formulations

The two-layer system of Figure 1 cannot cycle when the interfacial mixing is by salt fingers obeying the laboratory flux laws. However, the applicability of these flux laws to

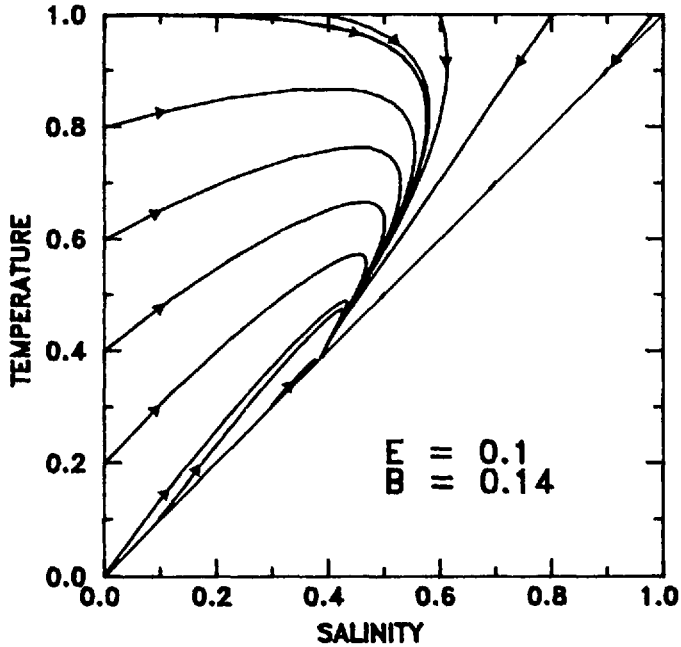


Figure 11. Solutions of (3.3) on the $T$-$S$ phase plane for a situation in which all initial conditions lead to overturning, followed by a limit cycle involving periodic overturning of the top layer into the lower layer. (Kelley $C(R_\rho)$, Kunze $\gamma(R_\rho)$). This appears to be the only way in which the salt finger system can exhibit a limit cycle.

the ocean is in serious question, even if the thermocline consists of several steps rather than a single interface (Kunze 1987, Hebert, 1988). Also, we found in Section 3 that trying to apply the interfacial flux laws to oceanic scales assuming a single interface leads to extreme difficulties in scaling. It would be much more realistic to parameterize oceanic salt finger fluxes in terms of the large-scale gradients of $T$ and $S$ in a manner similar to that for mechanical turbulence, but taking account of the special properties of salt fingers. Little is known about oceanic salt fingers, due to a lack of direct observations of *in-situ* fluxes. However, we do know enough about salt fingers to take an intuitive guess at the form for a gradient-based parameterization of ocean fluxes, and we investigate the possibilities for oscillation in such a system.

The simplest way to incorporate one of the unique properties of salt finger fluxes is to assume equal eddy diffusivities for $T$ and $S$, but instead of the diffusivity being a function of Richardson number, we assume it to be a function of gradient density ratio:

$$R\rho = \frac{-\alpha \dfrac{\partial T}{\partial z}}{\beta \dfrac{\partial S}{\partial z}}. \tag{4.1}$$

The dimensional form of eddy diffusivity for heat and salt is:

$$K = K_0 A(R_\rho) \tag{4.2}$$

where $K_0 = 10^{-4}\,\mathrm{m^2\,s^{-1}}$ is a scale constant as in Section 2. The dimensional equations, nondimensionalization, and scales are as in Section 2, and the resulting dimensionless equations take the form:

$$\frac{dS}{dt} = E - AS \equiv P(S, T) \tag{4.3a}$$

$$\frac{dT}{dt} = B(1 - T) - AT \equiv Q(S, T) \tag{4.3b}$$

which is exactly as for 2.8, with the exception that $A = A(R_\rho)$, where $R_\rho = T/S$. Using Bendixson's theorem, we find that

$$F(S, T) = \left(\frac{\partial P}{\partial S} + \frac{\partial Q}{\partial T}\right)_{\text{equil}} = -(B + 2A). \tag{4.4}$$

So, when the diffusivity depends on $R_\rho$, the quantity $F$ cannot change sign, and no limit cycle is possible. This is in contrast to equal diffusivities which depend on the density difference $\rho$, for which a limit cycle can occur. Simply changing the diffusivities to depend on $S/T$ rather than $S$-$T$ makes it impossible for the system to cycle.

The parameterization 4.2 is unrealistic because the diffusivities for heat and salt are equal. This leads to a downgradient buoyancy flux, which requires an external source of potential energy. In fact, salt fingers release potential energy, using the energy released to drive the mixing. Stern (1967) devised a parameterization which elegantly and simply captured this aspect of salt fingers. The salt flux is parameterized by an eddy diffusivity, as before:

$$F_S = K_0 A(R_\rho) \frac{\partial S}{\partial z}$$

where we have again assumed that the salt diffusivity primarily depends on the density ratio. The heat flux is parameterized by relating it to the salt flux via a flux ratio, as in Section 3:

$$\alpha F_T = -\gamma(R_\rho)\, \beta F_S.$$

This is equivalent to a thermal eddy diffusivity equal to $\gamma/R_\rho$ times the salt diffusivity:

$$\alpha F_T = K_0 A(R_\rho)\, \gamma(R_\rho)\, \beta \frac{\partial S}{\partial z}. \tag{4.5}$$

The equations are again scaled as in Section 2 to yield the following set of dimension-

less equations:

$$\frac{dS}{dt} = E - A(R_\rho)\, S \equiv P(S, T) \tag{4.6a}$$

$$\frac{dT}{dt} = B(1 - T) - A(R_\rho)\, \gamma(R_\rho)\, S \equiv Q(S, T). \tag{4.6b}$$

Computing the quantity used in Bendixson's theorem, we find

$$F(S, T) = \left(\frac{\partial P}{\partial S} + \frac{\partial Q}{\partial T}\right)_{\text{equil}} = -B + (R_\rho - \gamma)\, A' - (1 + \gamma')\, A. \tag{4.7}$$

This equation is closely analogous to 3.6, with $A(R_\rho)$ playing the role of $C$, and $\gamma$ playing itself. The only real change is the factor 4/3 in 3.6 has changed to 1 to reflect the single power of $S$ in the flux laws of this section. Since the first two terms are always negative, the only way for $F$ to change sign and allow a limit cycle is for $\gamma' < -1$. This also mirrors the result of Section 3.

The equilibrium points of 4.6 are $\overline{S} = E/A$, and $\overline{T} = \{1 + \gamma A/(R\rho B)\}^{-1}$ and the $R_\rho$ value at which these occur can be found from the equation

$$\frac{\overline{S}}{\overline{T}} = R_\rho^{-1} = \frac{E}{A}\left(1 + \frac{\gamma A}{R_\rho B}\right). \tag{4.8}$$

Defining $Y = R_\rho E/A(R_\rho)$, such that $Y$ increases monotonically with $R_\rho$, 4.8 becomes

$$Y = 1 - \frac{E}{B}\gamma(Y). \tag{4.9}$$

In this form, 4.9 can be solved graphically in much the same manner as in Section 3. The left side of 4.9 is plotted as a straight line of slope 1, the right side is plotted as a function of $Y$, and intersections of the two curves indicate values of $Y$ corresponding to solutions of 4.9. For constant $\gamma$, the rhs of 4.9 is constant, and since the lhs is monotonically increasing with $Y$, there is only one intersection. For nonconstant $\gamma$, recalling the $\gamma$ curves up toward 1 sharply toward 1 as $R_\rho$ nears 1 (recall Fig. 3), the rhs of 4.9 is approximately constant at large $Y$, but dips down sharply as $Y$ approaches $E$ from above. So for $E \approx 1$ and $B \leq E$, there are two solutions to 4.9. As in Section 3, the one at large $Y$ (and $R_\rho$) corresponds to the one for constant $\gamma$, and the one at small $Y$ is due to variable $\gamma$. Using the same methods as in Section 3, it can be shown that the equilibrium point at large $R_\rho$ is a stable node or spiral, and the one at small $R_\rho$ is a saddle. Using Poincare's index theorem and Bendixson's theorem as in Section 3, we argue that no limit cycle can occur.

Thus, the system 4.6 is analogous to 3.3, except that the power 4/3 is replaced by 1. This makes for some changes in the algebra, but no qualitative changes. The main

result, that no limit oscillation can occur under salt finger flux parameterizations, is the same for both systems.

## 5. Discussion

Welander (1982) and Stommel (1986) found that a two-layer "ocean" driven by evaporation and heating at the surface, and run down by turbulent mixing at the interface between the layers, can have an unsteady limit cycle in which the mixing is alternately less than and greater than the forcing. The key feature which allows a cycle is that the mixing changes strength rapidly at a finite density difference. In Sections 3 and 4 of this paper, we found that when the mixing between the two layers is parameterized in a way suitable for salt fingers, no cycle is possible.

What is the difference between mixing by turbulence and by salt fingers which allows a limit cycle in the former case, but not the latter? The evaporation and heating are parameterized in such a way that the forcing can cause density to increase or decrease, depending on the position on the ($T$, $S$) plane. The effect of salt finger and turbulent mixing is similar in that both cause a decrease in $T$ and $S$, and both become much stronger as the density contrast between the layers becomes small. Turbulent mixing has a negative buoyancy flux (a gain of potential energy), while salt fingers release potential energy via a positive buoyancy flux. This serves to change the slope of the trajectories, but doesn't appear to lead to any qualitative differences. The difference between salt finger and turbulent mixing that seems to be responsible for the different behavior is that turbulent mixing depends on the density difference of the top and bottom layers via the Richardson number, while salt finger mixing depends on the density ratio. On the $T$-$S$ phase plane, turbulent mixing is equally strong along lines of constant $S$-$T$ (distance from the $S = T$ boundary), while salt finger mixing coefficients are constant along lines of constant $T/S$, corresponding to constant angle. We have failed to see why such a subtle change in mixing parameterization can lead to such a drastic change in behavior of the Stommel/Welander model.

In the main thermocline of the subtropical oceans, where evaporation exceeds precipitation, both salt finger mixing and mixing by mechanical turbulence are likely to be occurring. A cycle can occur only if turbulent mixing dominates, and if the dependence of mixing rate on stratification is sufficiently strong. Observational evidence is lacking for this dependence, and so a cycle is not expected to occur even if turbulent mixing is dominant.

*Acknowledgments.* The authors are supported by the Natural Sciences and Engineering Research Council of Canada.

## APPENDIX

### Theorems useful for two-variable autonomous systems

Autonomous two-variable systems of equations are discussed in many textbooks of mathematical techniques for engineers and scientists. In this Appendix, we review

some qualitative techniques which allow the general nature of solutions to be deduced, and describe three theorems which are used in the body of this paper to deduce the existence or nonexistence of a limit cycle. The authors' favorite treatment of the qualitative techniques, and of the theorems, is in part 1 of Minorsky (1962), although the theorems are also discussed in Davis (1962).

Consider the system of equations:

$$\frac{dS}{dt} = P(S, T) \tag{A1a}$$

$$\frac{dT}{dt} = Q(S, T) \tag{A1b}$$

in which $P$ and $Q$ are analytic (differentiable) functions of $T$ and $S$, but not explicitly functions of time. This system is called autonomous. The vector field $(P, Q)$ is thus well defined, and describes the "flow" of the solutions in a manner analogous to the flow of fluid particles in a velocity field. The solutions $S(t)$, $T(t)$ of Eqs. (A1) may be conveniently represented as trajectories on the $(S, T)$ phase plane, since for autonomous systems time is simply a parameter (i.e., starting an integration at a later time will simply delay the solution by a constant time). These trajectories may in principle be found by eliminating time from A1, and integrating. They have local slope $dT/dS = Q/P$. The only places this procedure will fail are at *critical points*, which are points where both $P$ and $Q$ are zero, and the slope is indeterminate. These points correspond to stagnation points in the fluid flow analogy. Trajectories passing through critical points are not uniquely defined; there can be an infinite number passing through each critical point, each solution taking an infinite time to do so.

The pattern of trajectories in the vicinity of a critical point is straightforward to analyze, by moving to an origin centered on the critical point, and expanding A1 in a first-order Taylor series. The resulting system:

$$\frac{d(\delta S)}{dt} = \frac{\partial P}{\partial S}\delta S + \frac{\partial P}{\partial T}\delta T \tag{A2a}$$

$$\frac{d(\delta T)}{dt} = \frac{\partial Q}{\partial S}\delta S + \frac{\partial Q}{\partial T}\delta T \tag{A2b}$$

where the partial derivatives are evaluated at the origin, is a linear, $2 \times 2$ system describing the evolution of perturbations about the critical point. The eigenvalues (Eq. 3.8) and eigenvectors of the $2 \times 2$ matrix uniquely determine the "flow" of the trajectories passing through and near the critical point, and hence uniquely define the type of point (Minorsky, 1962, Ch. 1). The type may be: (1) a saddle [two purely real eigenvalues of opposite sign], in which "flow" lines resemble, with some distortion, the classic strain field, (2) a node [two real eigenvalues, one positive and one negative],

which resembles a sink or source and is sometimes called exactly that, (3) a center, which is analogous to a vortex [two imaginary eigenvalues], and (4) a focus (also called a spiral), in which "flow" lines swirl in or out from the critical point [complex conjugate eigenvalues].

Trajectories are analogous to streaklines in a (possibly nonvolume conserving) flow described by $(u, v) = (P, Q)$, and their properties may be rationalized by thinking of them as such. The fact that trajectories do not begin or end except at boundaries or critical points, and that they do not cross (for then they would be nonunique), is extremely useful. For a given system, a qualitative picture of the phase plane may be gained by analyzing the type and position of all critical points, and trying to determine the connections between them (i.e., the trajectories which connect from one critical point to another). Even if the position (but not the type) of the critical points is changed, the topology of the phase plane ("flow field") will remain the same. However, when a change in parameter values causes a critical point to change type, the topology can change.

Often, a nonlinear autonomous sytem will exhibit self-sustained, finite-amplitude oscillations: this is called a *limit cycle*. Three theorems which are very useful in determining the existence or nonexistence of a limit cycle are described in the remainder of this Appendix.

**Poincare's index theorem**

This theorem establishes necessary conditions for a limit cycle to exist, using the geometry of how trajectories fan out or in from critical points and limit cycles. The proof uses residue calculus and the fact that arctan $(P/Q)$ is an analytic function of $(S, T)$. The *index* of a closed curve C is defined as the number of revolutions the vector $(P, Q)$ describes (measured positive counterclockwise) as $C$ is traversed once in the counterclockwise direction. The index of a closed curve containing no critical points is zero. This is topologically equivalent to a closed curve in a uniform vector field: as the curve is traversed, the vector does not change direction, giving a zero index. Similarly, a curve surrounding a saddle can be seen to have index $-1$, meaning that the vector tangents rotate clockwise exactly once in traversing the curve. A curve surrounding a node, focus or centre has index $+1$. Davis (1962, p. 353) sketches these situations clearly. Analogous to residue calculus, the curve $C$ can be moved or distorted without changing its index, so long as the curve continues to surround the same critical points. Similarly, the index of any closed curve is determined by the sum of the indices of the critical points inside the curve. Now consider a closed trajectory, and let $C$ coincide with the trajectory. As $C$ is traversed, the tangent to $C$ rotates once, so the index of the closed trajectory is $+1$. This leads to the theorem:

*The number of nodes plus centers plus foci contained within any closed trajectory must exceed by one the number of saddles.*

The theorem can be used to locate the possible areas through which a limit cycle may pass, and if the conditions cannot be met, to prove that a cycle cannot exist.

**Bendixson's first theorem**

This theorem also establishes necessary conditions for the existence of a limit cycle. Assume there is a closed trajectory $C$. By A1, $C$ is everywhere tangent to the vector field $(P, Q)$, so that on $C$:

$$\frac{dS}{dT} = \frac{P}{Q}, \text{ so that}$$

$$\oint (PdT - QdS) = 0$$

since the integration is around the closed curve. Then, using Green's theorem,

$$\oint \left(PdT - QdS\right) = \int\int_D \left(\frac{dP}{dS} + \frac{dQ}{dT}\right) = 0.$$

Where the area $D$ is that inside the curve $C$. Since the area integral above must be zero, the quantity in brackets must either be zero or change sign. The first possibility can be eliminated because it would correspond to a uniform flow field, which cannot be bounded by a limit cycle. Therefore:

*The quantity* $\left(\frac{dP}{dS} + \frac{dQ}{dT}\right)$ *must change sign within a closed trajectory.*

This theorem is used in practice to find conditions under which a limit cycle is impossible.

**The Poincare-Bendixson theorem**

This theorem gives sufficient conditions for a limit cycle to exist, and so is useful for proving conditions under which a limit cycle must occur. Its proof is related to Poincare's index theorem, relying on the topology of how trajectories cross a closed curve. The theorem states:

*If a trajectory C remains in a finite domain D without approaching any critical points (singularities), then C is either a closed trajectory or approaches one.*

To paraphrase: if we can find a region bounded entirely by inward-pointing trajectories which has no singularities within that region, then all trajectories entering the region cannot approach steady state and must enter a limit cycle. The practical difficulty is usually in finding such a region.

In this paper, the domain is the entire $T$-$S$ phase plane, and the argument relies on trajectories all entering the domain from the boundaries. Then if all singular points are unstable nodes or foci, no trajectories can approach them, and all trajectories entering the domain (i.e., all initial conditions) must approach a limit cycle.

## REFERENCES

Davis, H. T. 1962. Introduction to Nonlinear Differential and Integral Equations, Dover Publications, Inc., NY, 352–355.

Gargett, A. E. 1984. Vertical eddy diffusivity in the ocean interior. J. Mar. Res, *42*, 359–393.

Gargett, A. E. and G. Holloway. 1984. Dissipation and diffusion by internal wave breaking. J. Mar. Res., *42*, 15–27.

Hamilton, James M., M. R. Lewis and B. R. Ruddick. 1989. Vertical fluxes of nitrate associated with salt fingers in the world's oceans. J. Geophys. Res., *94*, 2137–2145.

Haney, R. L. 1971. Surface thermal boundary conditions for ocean circulation models. J. Phys. Oceanogr., *1*, 241–248.

Hebert, D. 1988. Estimates of salt finger fluxes. Deep-Sea Res., *35*, 1887–1901.

Henderson-Sellers, B. 1982. A simple formula for vertical eddy diffusion coefficients under conditions of nonneutral stability. J. Geophys. Res., *87*, 5860–5864.

Huppert, H. 1972. On the stability of a series of double-diffusive layers. Deep-Sea Res., *18*, 1005–1021.

Kelley, D. 1986. Oceanic thermohaline staircases. Ph.D. thesis, Dalhousie University, Halifax, N.S., Canada.

Kunze, E. 1987. Limits on growing, finite-length salt fingers: a Richardson number constraint. J. Mar. Res., *45*, 533–556.

Minorsky, N. 1962. Nonlinear Oscillations. D. van Nostrand Co., Inc., Princeton, 714 pp.

Munk, W. H. 1981. A survey of internal waves and small-scale processes, *in* Evolution of Physical Oceanography, B. A. Warren and C. Wunsch, eds., MIT Press, Cambridge, MA, 264–291.

Munk, W. H. and E. R. Anderson. 1948. Notes on a theory of the thermocline. J. Mar. Res., *7*, 276–295.

Pacanowski, R. C. and S. G. H. Philander. 1981. Parameterization of vertical mixing in numerical models of tropical oceans. J. Phys. Oceanogr., *11*, 1443–1451.

Peters, H., M. C. Gregg and J. M. Toole. 1988. On the parameterization of equatorial turbulence. J. Geophys. Res., *93*, 1199–1218.

Schmitt, R. W. 1981. Form of the T-S relationship in the central water: evidence for double-diffusive mixing, J. Phys. Oceanogr., *11*, 1015–1026.

Schmitt, R. W., P. S. Bogden and C. E. Dorman. 1989. Evaporation minus precipitation and density fluxes for the North Atlantic. J. Phys. Oceanogr., *19*, 1208–1221.

Stern, M. E. 1967. Lateral mixing of water masses. Deep-Sea Res., *14*, 747–753.

Stommel, H. 1961. Thermohaline convection with two stable regimes of flow. Tellus, 13, 224–228.

——1986. A thermohaline oscillator. Ocean Modelling, *72*, 5–6. (unpublished manuscript).

Turner, J. S. 1973. Buoyancy Effects in Fluids, Cambridge University Press, Cambridge, U.K. 368 pp.

Welander, P. 1982 A simple heat-salt oscillator. Dyn. Atmos. Oceans, *6*, 233–242.

Received: *6 April, 1989;* revised: *9 August, 1989.*